Supporting Information

Sharma et al. 10.1073/pnas.0901631106

SI Text

Isolation of highly-purified ribosomes from *Leishmania* mitochondrion has been a challenge for many years. Because of its significantly greater proportion of protein and lower proportion of rRNA (1, 2), the Lmr is much more labile than are cytoplasmic or mammalian mitochondrial ribosomes. Because of the lower proportion of rRNA, cryo-EM images of the Lmr have poorer contrast at close-to-focus values as compared with what is achievable for other ribosomes studied with the cryo-EM technique. Furthermore, the 2 subunits of the Lmr appear to dissociate readily to form their homodimers (1, 2), which sediment close to the 50S peak and cause an additional heterogeneity issues. We removed homodimers of the Lmr subunits through repeated sucrose-density gradient centrifugation; however, the low contrast of the images and the inherent conformational heterogeneity both pose challenge in acquisition of a high-resolution 3D cryo-EM map for the 50S Lmr. The fact that from initially-picked 185,413 images only 53,475 images could be included in the reconstruction of the 14-Å resolution map partly attributes to the above-mentioned inherent heterogeneity in the Lmr.

To rule out a possible reference bias in overall similarity of the Lmr map to that of a bacterial ribosome map, we used 2 other references separately for initial alignments: (*i*) the mammalian 55S mitochondrial ribosome map (3) and (*ii*) a map of the ratcheted *E. coli* 70S·EF-G complex (4). Although use of the 55S mitochondrial ribosome reference failed to produce convergence of the Lmr data, the map resulting from use of 70S·EF-G reference did not show any density corresponding to large EF-G moiety that was associated with the reference. Both of these results, the previous 2D analysis (1), and the fact that a significant proportion (≈45%) of the missing eubacterial rRNA segments (e.g., helix 44 of the SSU rRNA) are not compensated by densities in the cryo-EM map of Lmr, rule out any reference bias.

1. Maslov DA, et al. (2006) Isolation and characterization of mitochondrial ribosomes and ribosomal subunits from *Leishmania tarentolae. Mol Biochem Parasitol* 148:69–78.
2. Maslov DA, et al. (2007) Proteomics and electron microscopic characterization of the unusual mitochondrial ribosome-related 45S complex in. *Leishmania tarentolae. Mol Biochem Parasitol* 152:203–212.
3. Sharma MR, et al. (2003) Structure of the mammalian mitochondrial ribosome reveals an expanded role for its component proteins. *Cell* 115:97–108.
4. Datta PP, Sharma MR, Qi L, Frank J, Agrawal RK (2005) Interaction of the G′ domain of elongation factor G and the C-terminal domain of ribosomal protein L7/L12 during translocation as revealed by cryo-EM. *Mol Cell* 20:723–731.
5. de la Cruz V, Lake JA, Simpson AM, Simpson L (1985) A minimal ribosomal RNA: Sequence and secondary structure of the 9S kinetoplast ribosomal RNA from *Leishmania tarentolae. Proc Natl Acad Sci USA* 82:1401–1405.
6. Smith TF, Lee J, Gutell RR, Hartman H (2008) The origin and evolution of the ribosome. *Biol Direct* 3:16.
7. de la Cruz V, Simpson A, Lake J, Simpson L (1985) Primary sequence and partial secondary structure of the 12S kinetoplast (mitochondrial) ribosomal RNA from *Leishmania tarentolae*: Conservation of peptidyl-transferase structural elements. *Nucleic Acids Res* 13:2337–2356.
8. Wimberly BT, et al. (2000) Structure of the 30S ribosomal subunit. *Nature* 407:327–339.
9. Ban N, Nissen P, Hansen J, Moore PB, Steitz TA (2000) The complete atomic structure of the large ribosomal subunit at 2.4-Å resolution. *Science* 289:905–920.
10. Harms J, et al. (2001) High-resolution structure of the large ribosomal subunit from a mesophilic eubacterium. *Cell* 107:679–688.
11. Yusupova G, Jenner L, Rees B, Moras D, Yusupov M (2006) Structural basis for messenger RNA movement on the ribosome. *Nature* 444:391–394.

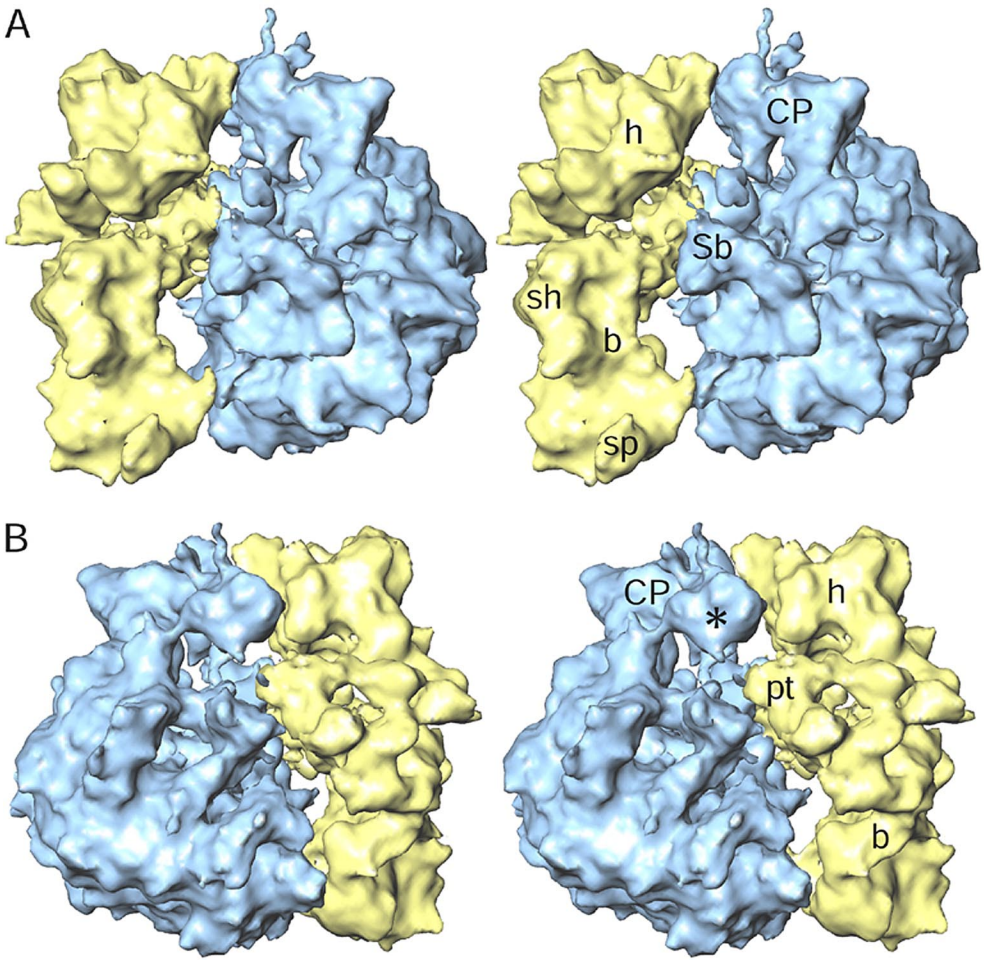

Fig. S1. Stereo representation of the cryo-EM structure of the Lmr. (*A*) A side-by-side view, showing the shoulder (sh) side of the 28S SSU (yellow), and the L7/12 protein-stalk base (Sb) side of the 40S LSU (blue). (*B*) Another side-by-side view, in which the Lmr has been rotated by ≈180° around a virtually vertical axis, shows the platform (pt) side of the SSU and L1-protein (*) side of the LSU. b, body; h, head; sp, spur; CP, central protuberance.

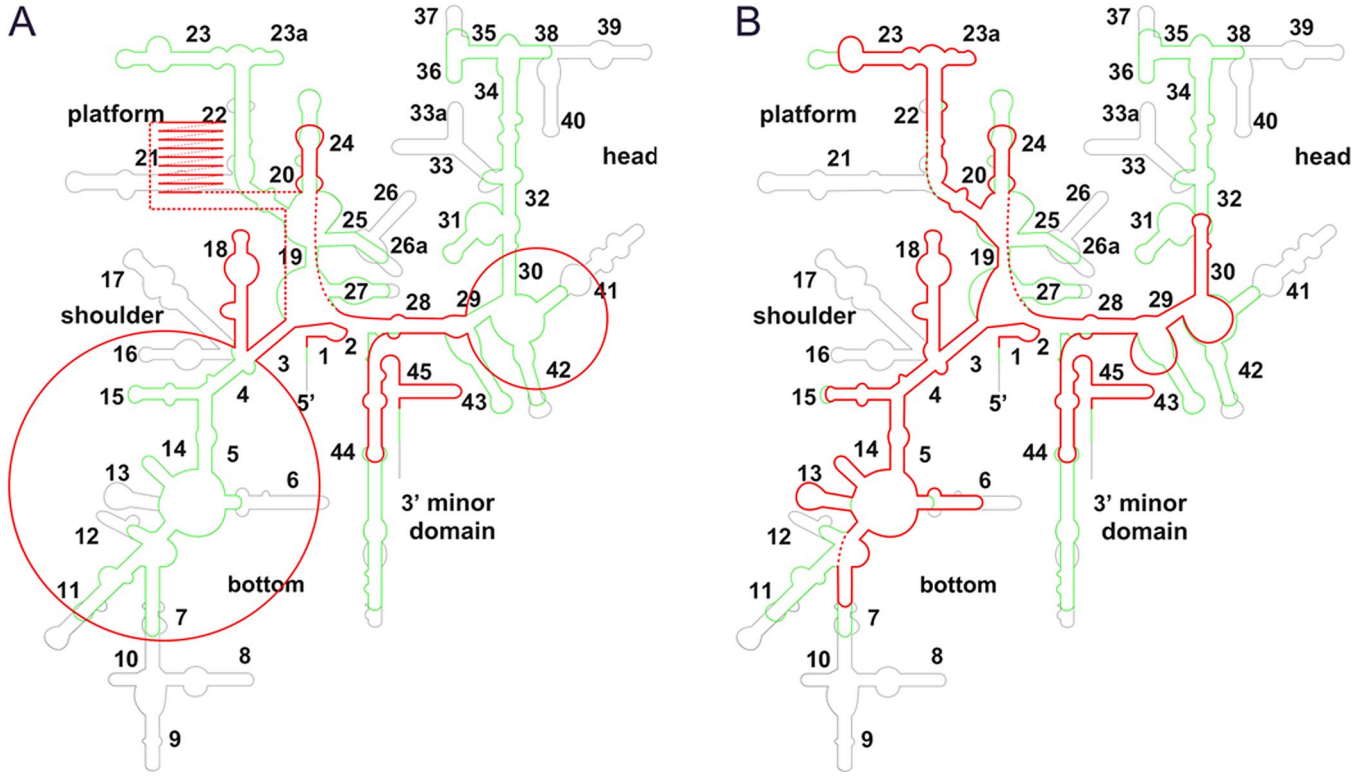

Fig. S2. Line diagram showing a comparison of secondary structures of rRNAs between bacterial (16S, gray), mammalian mitochondrial (12S, green), and *L. tarentolae* mitochondrial (9S, red) ribosomal SSUs. (*A*) Secondary structure of the 9S rRNA as was available before the present study (5, 6). (*B*) Secondary structure derived in the present study. Dashed lines in *B* indicate unassigned segments of rRNA.

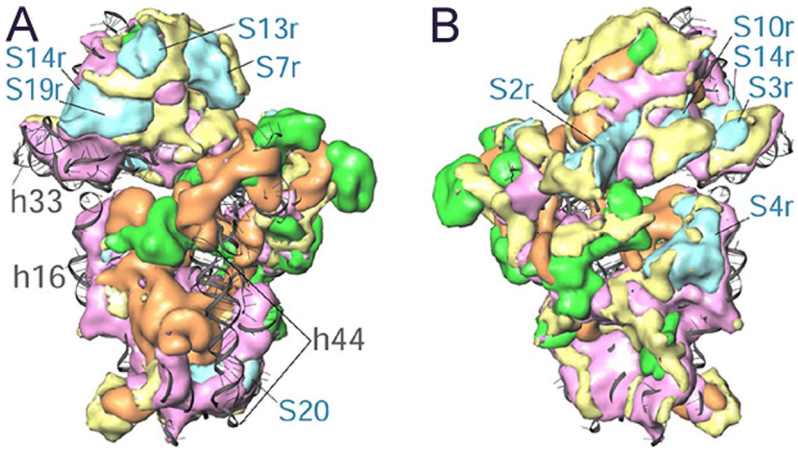

Fig. S3. Superposition of the nonconserved domains from the crystallographic structure of the bacterial SSU rRNA [gray ribbons, rRNA (8)] onto the Lmr SSU map (solid surfaces). SSU map is shown from the interface (*A*) and solvent (*B*) sides. Conserved bacterial proteins are shown in green. Magenta and blue densities correspond, respectively, to Lmr-specific protein masses that compensate for missing segments of bacterial rRNA and proteins. Thus, the yellow regions represent the protein masses that do not compensate for any missing bacterial ribosomal components. Most missing eubacterial rRNA segments (see Fig. S2) can be matched to sites where densities are absent in our cryo-EM map, indicating the lack of compensation of those rRNA segments by any protein in the Lmr. Numbers prefixed with S represent the SSU proteins; numbers prefixed with h identify the rRNA helices; suffix r indicates Lmr-specific masses that replace corresponding eubacterial proteins.

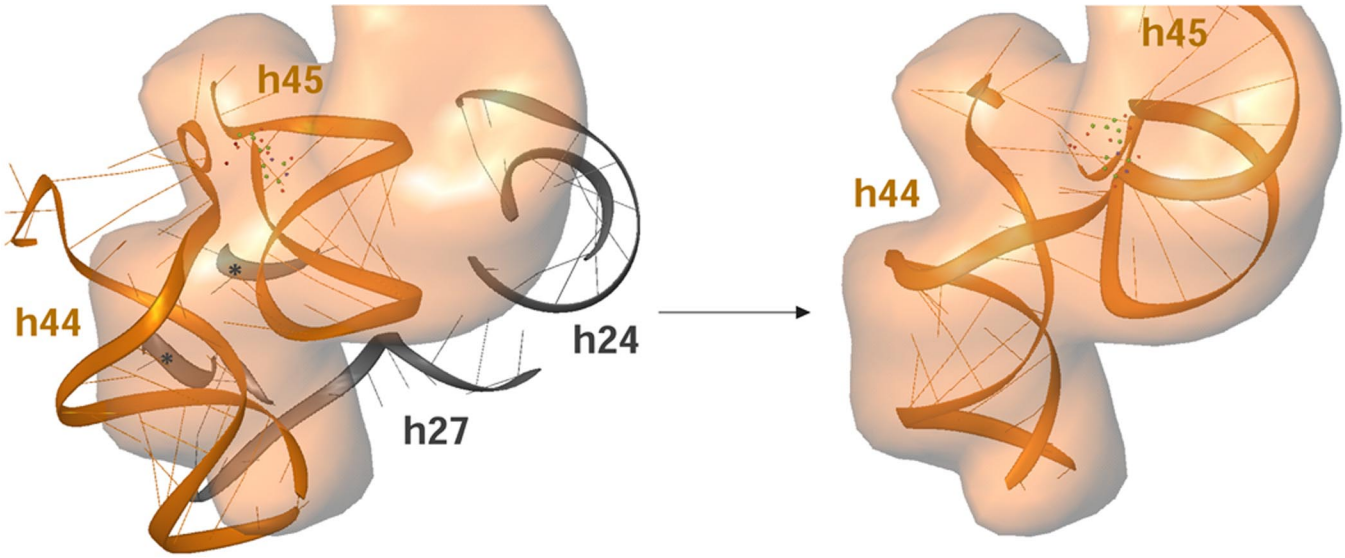

Fig. S4. Depiction of spatial movement of helix 44 (h44) and helix 45 (h45) in the Lmr SSU. Because of the absence of a part of h24 and most of h27, and segments of loops between helices h3 and h19 and between h19 and h20 (gray ribbons marked by *; see Fig. S2), all of which stack behind h44 and h45 in the eubacterial SSU structure (8), h44 and h45 shift more toward the platform in Lmr. (*Left*) Shown is the position of conserved segments of h44 and h45 (orange ribbons), based on rigid-body fitting of whole eubacterial SSU structure into the cryo-EM map (semitransparent orange) of Lmr SSU. (*Right*) Independent fittings of those helices are shown.

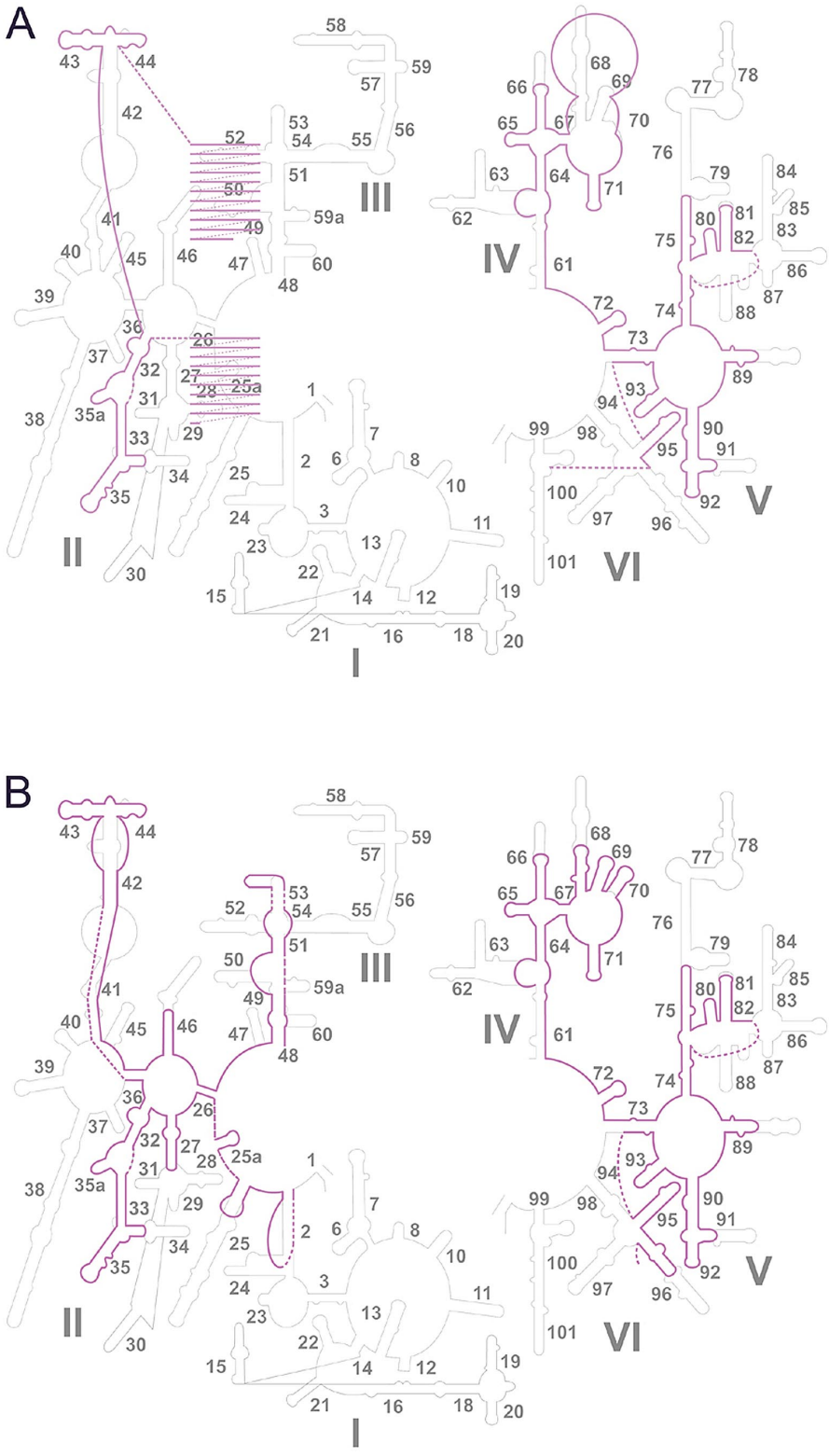

Fig. S5. Line diagram showing a comparison of secondary structures of rRNAs between bacterial (23S, gray), and *L. tarentolae* mitochondrial (12S, purple) ribosomal LSUs. (*A*) Secondary structure of the12S rRNA as was available before the present study (6, 7). (*B*) Secondary structure derived in the present study. Dashed line in *B* indicates unassigned segments of rRNA.

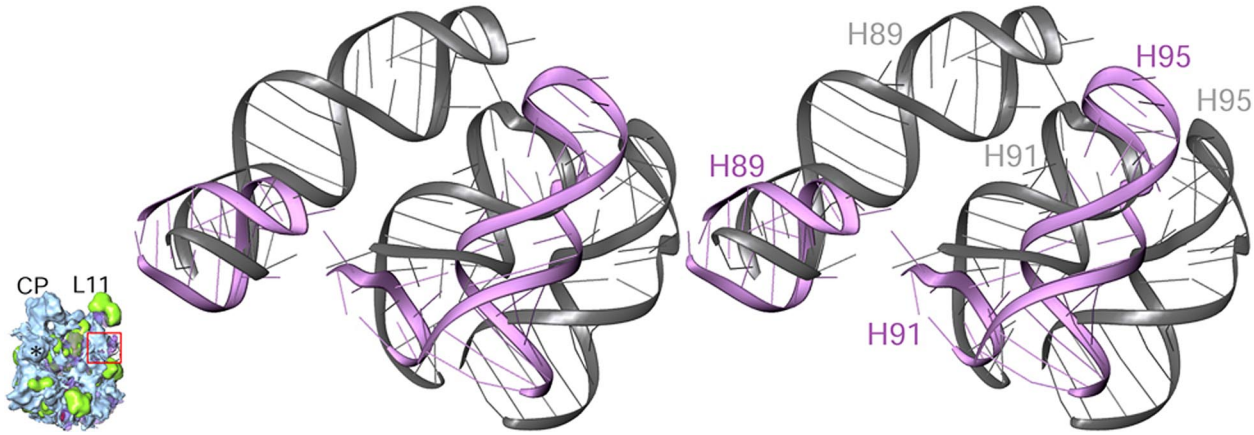

Fig. S6. Stereoview presentation of the spatial shift of helix 95 (H95, SRL) in the Lmr LSU. Most of bacterial 23S rRNA helix 91 (H91) and a major portion of helix 89 (H89) are absent in Lmr (pink) (see Fig. S5). Apparently, these deletions allow the spatial shift of SRL and bring it closer to the PTC in the Lmr.

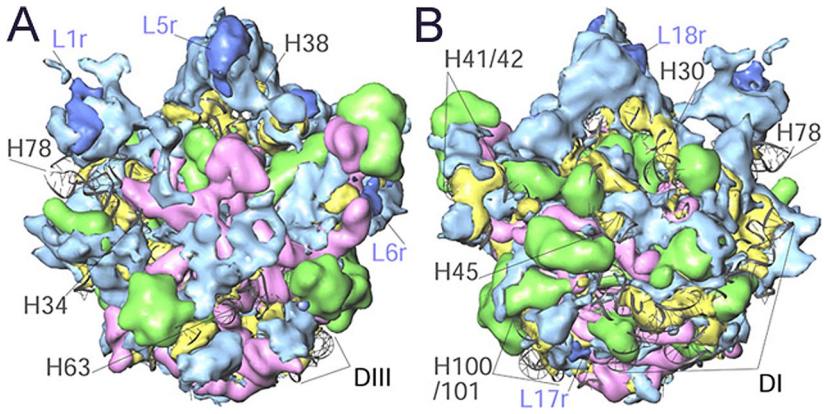

Fig. S7. Superposition of the nonconserved rRNA segments (gray ribbons) from the crystallographic structure of the bacterial LSUs (9, 10) onto the Lmr LSU map (solid surfaces) shown from the interface (*A*) and solvent (*B*) sides. Conserved bacterial proteins are shown in green. Yellow and dark blue densities correspond to Lmr-specific protein masses that compensate, respectively, for missing segments of bacterial 23S rRNA and proteins. Thus, the densities in light blue represent the protein masses that do not compensate for any missing bacterial ribosomal components. Numbers prefixed with L identify the LSU proteins; numbers prefixed with H identify the LSU rRNA helices. D I and D III, missing segments of domains I and III, respectively.

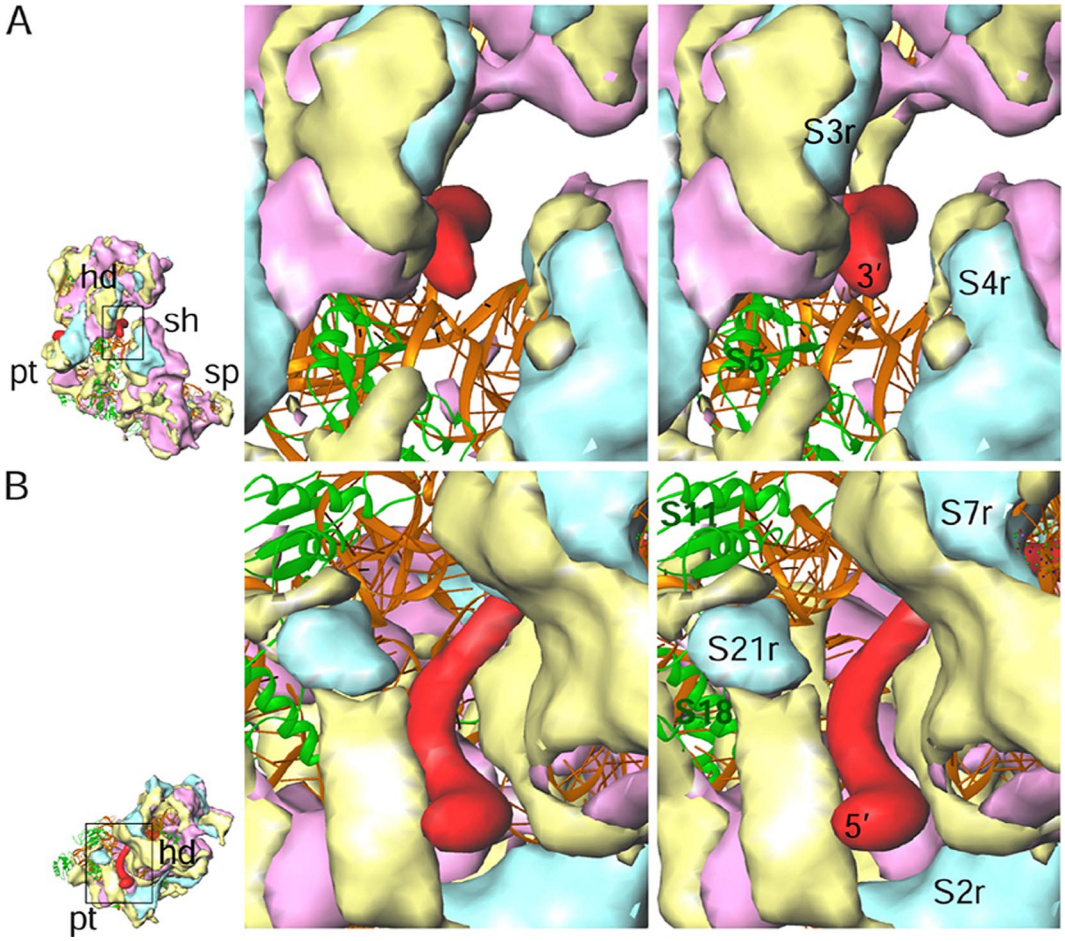

Fig. S8. Stereo representation of the topography of the mRNA path on the Lmr SSU. The path [based on the mRNA (red) position derived for the eubacterial ribosome in ref. 11] is composed principally of Lmr-specific proteins (solid masses, color codes as in Fig. S3). (*A*) mRNA entrance. (*B*) mRNA exit. The conserved SSU proteins are shown as green ribbons; and Lmr-specific protein masses (blue) that replace segments of bacterial proteins S2, S3, S4, S7, S19, and S21 are identified with suffix r. 3′ and 5′, 3′ and 5′ ends of the mRNA. Panels on the left show the orientation of the Lmr SSU; the boxed area has been enlarged for the stereo depiction.